# IR−UV Ion-Dip Spectroscopy of *N*-Benzylformamide Clusters: Stepwise Hydration of a Model Peptide

**E. G. Robertson, M. R. Hockridge, P. D. Jelfs, and J. P. Simons***

*Physical and Theoretical Chemistry Laboratory, South Parks Road, Oxford OX1 3QZ, U.K.*

*Received: August 2, 2000; In Final Form: October 16, 2000*

Fluorescence excitation, resonant two-photon ionization (R2PI) and IR−UV ion dip spectroscopy have been used to study conformers of *N*-benzylformamide (NBFA) and associated clusters including hydrates with up to $n = 3$ water molecules. The most stable conformer has a *trans* arrangement of the HNCO atoms. It is distinguished from the *cis* conformer by a higher frequency for the NH stretch (3478 $cm^{-1}$, compared to 3443 $cm^{-1}$) and lower frequency for the amide I overtone (3435 $cm^{-1}$, compared to 3465 $cm^{-1}$). The *cis* conformer forms cyclic H-bonded structures with one or two water molecules, binding via strong H-bonds to the neighboring C═O and NH groups. With the addition of a third water molecule, the cyclic water trimer binds to both these groups in preference to a linear chain of three waters. For *trans*-NBFA, a single water binds to the carbonyl group and is further stabilized by dispersive $CH\cdots O_{water}$ interactions. Two water molecules bind to the NH group instead and form a bridge to the $\pi$-system of the aromatic ring. A heterodimer species is also observed, composed of *cis*- and *trans*-NBFA. It is stabilized by $NH_{trans}\cdots O{=}C_{cis}$ and $NH_{cis}\cdots\pi_{trans}$ H-bonds, which give rise to shifts in the NH stretch frequency of −102 and −28 $cm^{-1}$, respectively. Flexibility of the amide side chain plays a key role in promoting additional $CH\cdots O_{water}$ interactions in these clusters. When compared to the unsolvated conformers, some of the clusters exhibit considerable distortion in the dihedral angle $\tau_1$ ($C_2C_1C_\alpha N$) and in $\tau_2$ ($C_1C_\alpha NC$), equivalent to the Ramachandran angle $\phi$ in proteins. Solvation also affects the photophysics of NBFA, as the clusters show normal fluorescence behavior while the $S_1$ states of the isolated molecules are affected by a competing, nonfluorescent decay process.

## 1. Introduction

The structural, physical and biological properties of proteins are crucially dependent on their hydrogen bonded interactions, particularly those involving the amide NH and CO groups. The most important of these are the NH···OC bonds which govern secondary structure, but interactions with water also warrant special attention. Water is important not only as the bulk solvent surrounding proteins, but as a chelating ligand found in specific sites in the interior. Raman and IR techniques are well suited to probing these interactions, given the sensitivity of vibrational modes to small changes in bonding. The conformation and solvation dependence of amide vibrations has particular importance given the widespread use of IR and Raman spectroscopy to examine secondary structure in peptides.[1]

The technique of IR−UV ion depletion has a valuable contribution to make, as it allows the IR spectrum to be measured separately for each species present in the jet expansion.[2,3] Not only can different conformers be compared, but size-selected hydrated clusters stabilized in a very specific geometry may also be examined. In this way the consequences of stepwise solvation may be explored free from bulk solvent effects. Spectral shifts in OH and NH frequencies provide an excellent diagnostic for the presence and strength of specific H-bonded interactions. In this laboratory, it has been applied to the study of conformation and hydration in 2-phenylethanol,[4] benzyl alcohol,[5] phenylalanine,[6] and the adrenaline analogues 2-amino-1-phenylethanol,[7] ephedrine, pseudoephedrine,[8] norephedrine and α-(methylaminomethyl) benzyl alcohol.[9]

The first amide studied via IR−UV techniques was 2-pyridone,[10,11] a cyclic, aromatic amide with the geometry constrained so that NH is *cis* to the CO group. This arrangement allows a water molecule to form hydrogen bonds with both groups simultaneously. High-resolution electronic spectroscopy of deuterated isotopomers, revealed the changes in bond lengths resulting from H-bond formation[12] and IR−UV experiments measured the red-shifts in the NH and CO stretch vibrations.[10] Most recently, IR−UV ion depletion spectroscopy has been used to study *N*-phenylformamide (NPF) and its hydrated clusters in the ground and excited ($S_1$) electronic states.[13] Their NH stretch bands readily differentiate *cis* (3441 $cm^{-1}$) and *trans* (3463 $cm^{-1}$) isomers. Clusters of *trans*-NPF with 1 or 2 water molecules show nearly equal preference for binding to the NH and CO sites. A further cluster is assigned in which a chain of four water molecules form an H-bonded bridge between NH and CO. No water clusters of *cis*-NPF have been detected in 1-color R2PI spectra.[14,15]

With very few exceptions, the amide links within peptides have a *trans* arrangement. The work on NPF provided the first IR−UV data on clusters of a *trans*-amide. The present paper describes an investigation on the conformation and clusters of *N*-benzylformamide. The methylene spacer between the aromatic ring and the amide introduces the key element of flexibility into the side chain. The experimental and theoretical work presented here affords an opportunity to explore the preferences for water binding, the strength of H-bonded interactions and how are they affected by cooperation, the importance of side chain flexibility and the influence of hydration on the geometry and electronic structure of the host molecule.

* Corresponding author. Fax: +44 1865 275410. E-mail: jpsimons@physchem.ox.ac.uk.

10.1021/jp002788d CCC: $19.00 
Published on Web 11/29/2000

## 2. Analytical and Experimental Procedures

**2.1. Molecular Orbital Calculations.** Possible structures of *N*-benzylformamide (NBFA) and its hydrate and dimer clusters were explored by performing a series of ab initio molecular orbital calculations using Gaussian 94[16] as follows:

(i) A set of starting geometries was generated for NBFA and its clusters. The NBFA molecule was given a planar arrangement of the amide bond, allowing both *cis* and *trans* isomers, while the dihedral angles $\tau_1$ ($C_2C_1C_\alpha N$) and $\tau_2$ ($C_1C_\alpha NC$) were systematically varied. Optimized conformational structures were used as the starting point for 1:1 water clusters. A set of structures was then generated in which the water molecule was bound to the N−H hydrogen, or to "lone pair" sites of the carbonyl group. Initial structures for 1:2 water clusters were based on optimized 1:1 structures for the *cis* and *trans* isomers. Drawing on the NPF work,[14] the second water molecule was connected to the first and placed in such a way that it could interact with the ring or the side chain. In the initial 1:3 structures, either a "daisy chain" of waters linked the CO and NH groups, or two waters of a cyclic water trimer were bound to NBFA in a fashion similar to the preferred 1:2 clusters.

(ii) Each geometry was then submitted to full ab initio optimization followed by vibrational frequency calculation at the HF/6-31G* level of theory. In cases where only one of the hydrogen atoms of the water molecule was bound to the host, the other hydrogen atom was rotated stepwise by 120° about the molecular OH axis and the resulting structure re-optimized to find any further local minima.

(iii) Further optimizations and harmonic frequency calculations were carried out with density functional theory (DFT) using the Becke3-Lee−Yang−Parr functional and a basis set including diffuse functions (B3LYP/6-31+G(d)). B3LYP calculations using this particular basis set have been found to reproduce well the OH stretch frequencies of small water clusters[17] and have served as a benchmark for comparisons across a range of molecules and cluster species.[4−9,13] The monomer species were also optimized at the MP2/6-31G** level, while 1:1 hydrates and selected 1:3 hydrates were optimized at the MP2/6-31G* level. Only single point MP2/6-31G*//HF/6-31G* energies were calculated for the 1:2 and 1:3 hydrates due to computational expense. Where alternative structures were found, varying *only in the orientation of a nonbonded water H atom*, the one which is more stable at the MP2 level is presented.

(iv) For the 1:1 water clusters, basis set superposition errors (BSSE) were calculated to include the fragment relaxation energy.[18]

(v) Ground state (HF/6-31G*) structures were subsequently optimized for the first electronically excited singlet state, at the CIS/6-31G* level of theory, to yield sets of rotational constants for the electronically excited, $S_1$ state of each species, together with the magnitudes and directions of the $S_1 \leftarrow S_0$ transition moment (TM).

**2.2. LIF, Mass-Selected R2PI and IR−UV Ion Depletion Spectroscopy.** Jet-cooled *N*-benzylformamide (NBFA) was introduced into the interaction region through a pulsed nozzle helium expansion system with stagnation pressure 2−4 bar and sample temperature 400 K. When required, water vapor was incorporated into the gas flow via a bypass system. Mass-selected, one color R2PI spectra were recorded at low resolution (ca. 0.5 $cm^{-1}$) using a Nd:YAG-pumped, frequency-doubled dye laser (LAS) operating at wavelengths ca. 260−270 nm. The time delay between the signals to open the valve and to fire the laser was varied to optimize either monomer or cluster formation. Ion signals were detected via a differentially pumped time-of-flight mass spectrometer (R. M. Jordan). To record IR−UV ion depletion spectra, the dye laser was selectively tuned to probe each of the spectral features of interest (C, T, $Tw_1$ etc.) in the UV spectrum. IR radiation in the 2.6−3.2 $\mu$m region was generated using a $LiNbO_3$ crystal to difference frequency mix the fundamental of a seeded Nd:YAG laser with the output of a Continuum ND6000 dye laser, operating with LDS 765 dye. The IR beam had a typical energy of 2−4 mJ per pulse and was focused with a 25 cm focal length $CaF_2$ lens onto the jet, antiparallel to the UV probe laser. To measure vibrational spectra of species in their $S_0$ state, the depleting IR beam was scanned and timed to arrive ∼200 ns prior to the UV probe laser. To detect additional vibrations associated with the $S_1$ state, the two lasers were synchronized for simultaneous arrival. IR−UV holeburn spectra were recorded by scanning the UV laser while the IR laser was fixed to be resonant with a vibration of the selected species. Laser-induced fluorescence excitation (LIF) spectra were obtained using the frequency-doubled, excimer-pumped, dye laser output and substituting an optically filtered photomultiplier for the mass spectrometric detection system. The laser line width was narrowed to ca. 0.1 $cm^{-1}$ by an intracavity etalon when partially resolved rotational band contours were measured.

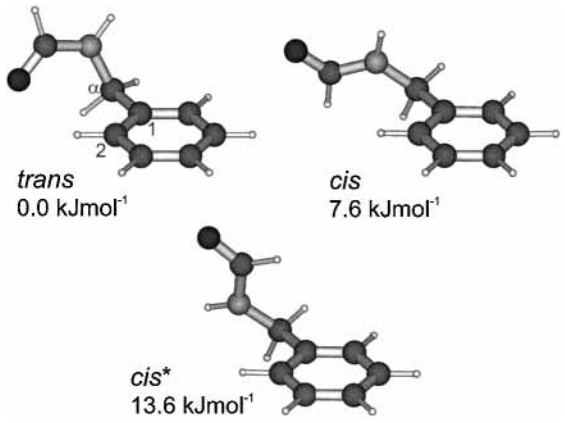


**Figure 1.** Conformers of NBFA predicted by MP2/6-31G** calculations with their relative energies. See Table 1.

## 3. Results

**3.1. Conformers of NBFA: Ab Initio Results.** Exploration of conformational space for the flexible side chain of NBFA at the HF/6-31G* level led to the discovery of just two stable structures, with *cis* and *trans* configurations of the amide group. Density functional calculations at B3LYP level with a 6-31+G* basis set gave a similar result. With the inclusion of electron correlation at the MP2/6-31G** level, however, a third potential minimum was observed: the alternative, higher energy *cis** conformer shown in Figure 1. The *trans* isomer is more stable than *cis*-NBFA at each level of theory, with the margin varying between 4 and 8 kJ $mol^{-1}$. The proximity of the oxygen atom to the ring in this conformer ($r_{CO\cdots HCring} = 245$ pm) suggests a van der Waals interaction may contribute to its stability. A summary of the ab initio data on NBFA molecular conformers is presented in Table 1.

**3.2. Conformers of NBFA: Experimental Assigments.** Mass-selected R2PI survey spectra of *N*-benzylformamide (NBFA) and associated clusters are shown in Figure 2. The upper trace shows the monomer mass channel in warm expansion conditions unfavorable to cluster formation. The strong feature labeled "T" appears at 37589 $cm^{-1}$, a frequency typical

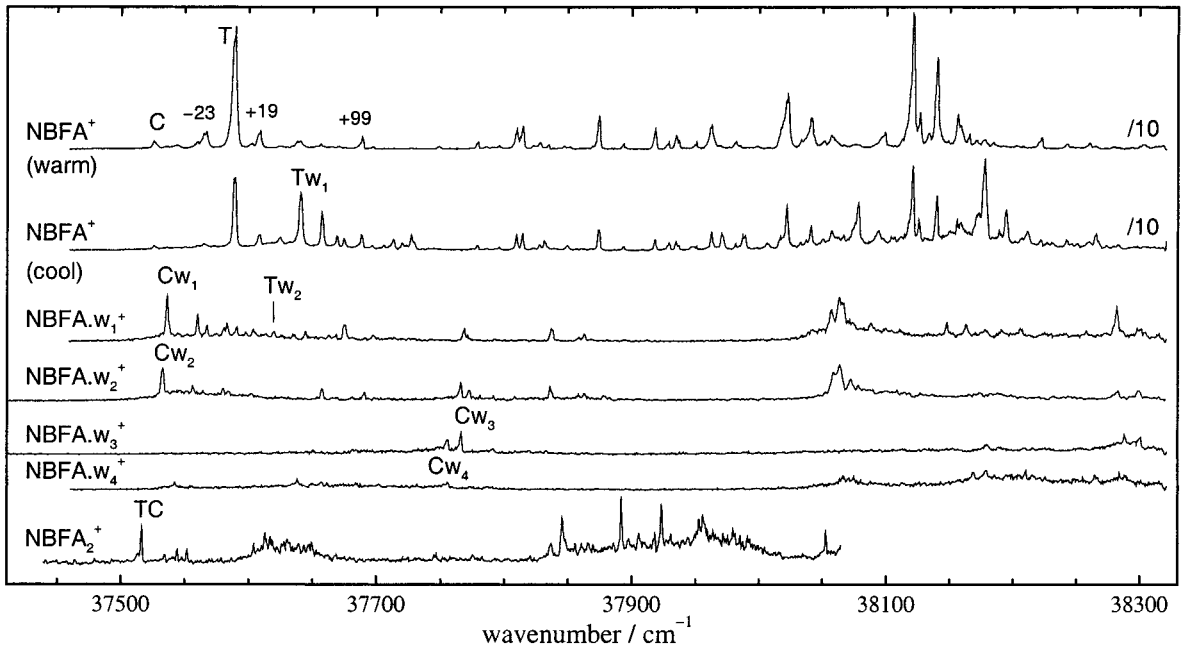


**Figure 2.** One-color R2PI spectra probing $NBFA^+$, $NBFA(H_2O)_n^+$, $n = 1-4$ and $NBFA_2^+$ mass channels. Excepting the top spectrum, the time delay between valve opening and laser firing was set to optimize cluster formation.

**TABLE 1: Ab Initio Results for NBFA Conformers**

| | *trans* | *cis* | *cis** |
|---|---|---|---|
| $E_{rel}$(HF)/kJ mol$^{-1}$ [a] | 0.0 | 5.3 | |
| $E_{rel}$(MP2)/kJ mol$^{-1}$ [b] | 0.0 | 7.6 | 13.6[d] |
| $E_{rel}$(B3LYP)/kJ mol$^{-1}$ [c] | 0.0 | 4.0 | |
| $\tau_1$ ($NC_\alpha C_1C_2$)/° | 71 | 43 | 43 |
| $\tau_2$ ($CNC_\alpha C_1$)/° | −92 | −115 | 63 |
| $\tau_3$ ($OCNC_\alpha$)/° | −6 | 177 | 171 |
| r ($C{=}O\cdots H-C_{ring}$)/pm | 245 | | |
| A″/MHz | 3111.6 | 3700.3 | 2978.5 |
| B″/MHz | 818.8 | 665.4 | 734.7 |
| C″/MHz | 691.7 | 581.0 | 677.2 |
| $\lvert R_e\rvert \times 10^{30}$/Cm[e] | 0.23 | 0.32 | 0.50 |
| $\mu_a^2$: $\mu_b^2$: $\mu_c^2$ [e] | 16:80:4 | 0:91:9 | 33:60:7 |
| $\theta_{elec}$/°[e] | -48 | -26 | 14 |

[a] HF/6-31G* including zero point correction scaled by 0.9. [b] MP2/6-31G** including scaled HF/6-31G* zero point correction. [c] B3LYP/6-31+G* including zero point correction. [d] zero point correction for *cis**-NBFA estimated from HF/6-31G* calculation for *cis* conformer. [e] CIS/6-31G*. $\theta_{elec}$ is defined as the angle between the short axis of the benzene ring perpendicular to the $C_1-C_\alpha$ bond and the transition moment. Positive angles represent a clockwise 'rotation' on the face of the ring, as viewed in Figure 1.

of $S_1 \leftarrow S_0$ origin transitions for molecules of this type ($C_6H_5$-$CH_2X$).[4−9,19] A number of weaker features appear in the same vicinity, shifted relative to "T" by −63 cm$^{-1}$ (C), −23 cm$^{-1}$, +19 cm$^{-1}$, +51 cm$^{-1}$ ($Tw_1$) and +99 cm$^{-1}$. In the region beyond 37700 cm$^{-1}$, every feature of significant intensity is accompanied by a weaker one 19 cm$^{-1}$ higher, and the intense vibronic features associated with excitation at +433 cm$^{-1}$ and of the ring mode at +532 cm$^{-1}$ show a further member of this short progression. The clear implication is that a low-frequency $S_1$ vibration of "T" is weakly allowed by Franck Condon considerations, so the +19 cm$^{-1}$ peak is assigned to a vibronic transition $\tau^1{}_0$. The second trace shows a spectrum recorded using a cold expansion, in which vibrational relaxation is more complete and the clusters are formed. The disappearance of the −23 cm$^{-1}$ peak suggests its assignment to a hot-band transition $\tau^0{}_1$. The dramatic growth of the +51 cm$^{-1}$ peak ($Tw_1$), in contrast, suggests a cluster that undergoes efficient fragmentation following resonant 1-color, 2-photon ionization. Only the −63 cm$^{-1}$ (C) and +99 cm$^{-1}$ peaks remain as candidates for alternative conformer origins.

IR−UV ion depletion spectra probing $S_1 \leftarrow S_0$ peaks C and T are shown in Figure 3. The IR spectrum generated by probing the +99 cm$^{-1}$ peak is identical to that of T, revealing that it is simply a vibronic feature of species T and not a separate conformer origin. The most prominent band in each spectrum (C, 3443 cm$^{-1}$; T, 3478 cm$^{-1}$) is readily assigned to the NH stretch of the amide group. The 35 cm$^{-1}$ difference allows C and T to be identified as the *cis* and *trans* conformers of NBFA by comparison with the B3LYP/6-31+G* calculations ($\Delta\nu$ = 25 cm$^{-1}$, see Table 2) and with NPF ($\Delta\nu$ = 22 cm$^{-1}$).[13] This is consistent with their relative intensities in the electronic spectrum: the dominant peak T belongs to the lowest energy conformer (*trans*). The absence of a third $S_1 \leftarrow S_0$ conformer origin is no surprise since *cis** is a high energy structure (+13.6 kJ mol$^{-1}$ relative to *trans*) with only a low barrier to prevent relaxation to the more stable *cis* conformer. In an earlier study of NBFA in $CCl_4$, two NH stretch bands at 3452 and 3418 cm$^{-1}$ were attributed to *trans* and *cis* conformers, respectively.[20] The 34 cm$^{-1}$ separation mirrors the present gas-phase results, as do the relative concentrations. In dilute solution of NBFA at 30 °C, the *cis*/*trans* ratio was 7% ± 2%, corresponding to $\Delta G$ = 6.7 ± 0.7 kJ mol$^{-1}$.

The IR spectra also contain a second, weaker feature (C, 3465 cm$^{-1}$; T, 3435 cm$^{-1}$), assigned to the carbonyl stretch (amide I) overtone. In the vapor-phase, room-temperature spectrum of NBFA, the fundamental of this mode is observed as an extremely intense band centered at 1730 cm$^{-1}$.[21] This may be considered as the frequency for *trans*-NBFA, since the populations found in the jet expansion derive from a warm stagnation region in which *cis*-NBFA contributes less than 10%. The anharmonicity for the amide I overtone of *trans*-NBFA may be estimated therefore at 25 cm$^{-1}$. If the anharmonicity is similar for *cis*-NBFA, its amide I fundamental might be expected at ca. 1745 cm$^{-1}$. These values are in excellent accord with the B3LYP/6-31+G* results: 1733 cm$^{-1}$ for *trans*-NBFA and 1743 cm$^{-1}$ for *cis*-NBFA. The corresponding frequencies at the HF/6-31G* level, 1749 and 1769 cm$^{-1}$, show a similar trend. It is

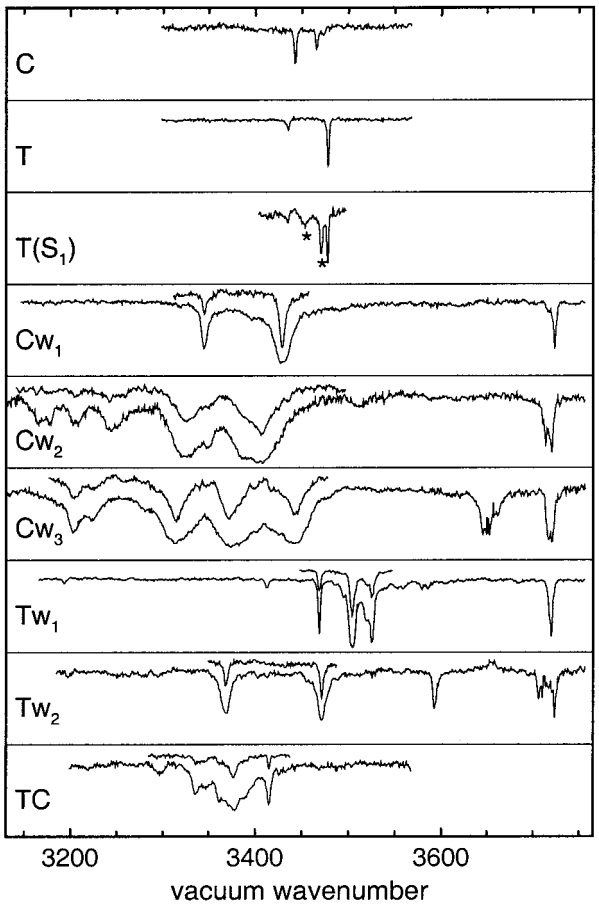


**Figure 3.** IR−UV ion depletion spectra of NBFA and associated clusters, probing the electronic origin bands C, T, $Cw_1$, $Cw_2$, $Cw_3$, $Tw_1$, $Tw_2$ and TC as labeled in Figure 2. The IR spectrum $T(S_1)$ was obtained with the IR and UV laser pulses arriving simultaneously. Most of the spectra were recorded with the $CaF_2$ lens at a distance 27 cm. Where two traces are shown, the upper one is a portion of the spectrum measured with the lens at a distance 32 cm to reduce the IR power density.

notable that the IR spectrum of *cis*-NPF is almost identical to *cis*-NBFA, with the NH stretch at 3441 $cm^{-1}$ and the amide I overtone at 3467 $cm^{-1}$.

Most of the spectra in Figure 3 are conventional IR−UV ion dip spectra, recorded with the IR laser fired ∼200 ns prior to the UV probe. The third spectrum was recorded by probing T while the IR and UV lasers were timed for simultaneous arrival. Additional features, marked *, arise which correspond to vibrations in the $S_1$ state. The NH stretch is red-shifted 7 $cm^{-1}$ from its $S_0$ position, and it appears that the amide I overtone is blue-shifted 18 $cm^{-1}$, both changes being consistent with a small degree of electron migration from the amide to the ring upon excitation. The 7 $cm^{-1}$ shift for the NH stretch is much less than was observed in NPF (48 $cm^{-1}$), reflecting the insulating effect of the methylene spacer between the amide and the ring.

Fluorescence excitation spectra of NBFA are shown in Figure 4. When fluorescence is detected in the interval from 90 to 190 ns after the UV laser pulse (upper trace), cluster features are evident but there is no signal from the monomer species T or C. This is unusual since most molecules of $C_6H_5CH_2X$ have fluorescence lifetimes of ca. 70 ns.[22] By setting the gate for fluorescence detection at 0−30 ns (lower trace), a small fluorescence yield is obtained for the *trans*-NBFA. By varying the timing for fluorescence detection, the lifetime of the $S_1$ state was determined to be ca. 20 ns. The short lifetime, together

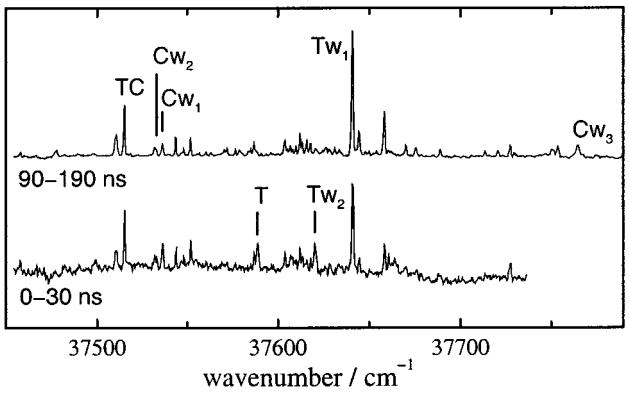


**Figure 4.** Fluoresence excitation spectra of NBFA, with gates for fluorescence detection set to 0−30 ns or 90−190 ns.

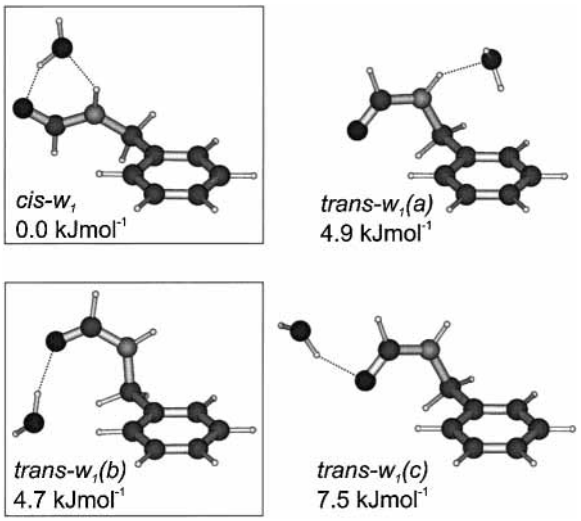


**Figure 5.** Ab initio structures (MP2/6-31G*) for 1:1 hydrates of NBFA, together with their relative energies. See Table 3. The enclosing boxes indicate structures that are assigned experimentally.

with the low fluorescence yield implies that a competing process such as nonradiative relaxation or triplet interconversion is depleting the $S_1$ state. The lifetime for this process, $\tau_n$, is ca. 20−25 ns, while the fluorescence lifetime $\tau_f$, estimated from the relative heights of T and $Tw_1$ is ca. 100−300 ns. CIS/6-31G* calculations of the $S_1$ states have been performed for NBFA conformers and some results are summarized in Table 1. The rotation of the $S_1 \leftarrow S_0$ transition moment away from the short axis of the ring, given by the value of $\theta_{elec}$ for each conformer, is not unusual for substituted benzenes of this sort. It is influenced both by electrostatic "through space" interactions with the side chain and by "through bond" factors such as distortion of the dihedral angle $\tau_1$ ($C_2C_1C_\alpha X$) away from 90°.[23] What is more unusual about the CIS data is that the magnitudes of the TMs are smaller than the typical values of ca. 1.0 × $10^{-30}$ C m.[19] The reliability of this aspect of the CIS calculation is not yet determined, but the present result is in accord with the experimental evidence of a longer fluorescence lifetime than 70 ns.

**3.3. NBFA$(H_2O)_{1,2}$: Ab Initio Results.** Structures of NBFA-$(H_2O)_1$ clusters optimized at the MP2/6-31G* level are shown in Figure 5. Their molecular parameters and binding energies (including zero point and BSSE corrections) are summarized in Table 3. The *cis* amide is able to bind water via hydrogen bonds to both NH and CO groups, resulting in an extremely stable complex with the greatest binding energy (35 kJ $mol^{-1}$).

**TABLE 2: Experimental and ab Initio Vibrational Wavenumbers of NBFA and Its Clusters**

| UV band probed | $\nu(S_1)/cm^{-1}$ | $\nu(S_0)/cm^{-1}$ | structure | mode description | freq[a]/$cm^{-1}$ | intensity/ km $mol^{-1}$ |
|---|---|---|---|---|---|---|
| C | | 3443 | *cis* | NH | 3494 | 21 |
| | | 3465 | | $2\nu_{C=O}$ | | |
| | | | | $\nu_{C=O}$ | 1743 | 424 |
| T | 3471 | 3478 | *trans* | NH | 3520 | 20 |
| | 3452 | 3435 | | $2\nu_{C=O}$ | | |
| | | 1730[19] | | $\nu_{C=O}$ | 1733 | 670 |
| $Tw_1$ | | 3469 | *trans*-$w_1$(b) | NH | 3515 | 16 |
| | | 3505/3525 | | OH··O═C | 3496 | 376 |
| | | 3720 | | free OH | 3727 | 91 |
| | | 3194 | | $2\nu_2$ of $H_2O$ | | |
| | | | *trans*-$w_1$(c) | NH | 3521 | 24 |
| | | | | OH···O═C | 3482 | 676 |
| | | | | free OH | 3723 | 110 |
| | | | *trans*-$w_1$(a) | NH···O | 3440 | 197 |
| | | | | OH···$\pi$ | 3624 | 48 |
| | | | | free OH | 3741 | 116 |
| $Tw_2$ | | 3368 | *trans*-$w_2$(a) | NH···water | 3369 | 395 |
| | | 3472 | | OH···water | 3432 | 494 |
| | | 3593 | | OH···$\pi$ | 3595 | 183 |
| | | 3709 | | free OH | 3723 | 128 |
| | | 3724 | | free OH | 3726 | 85 |
| $Cw_1$ | | 3345 | *cis*-$w_1$ | NH···water | 3369 | 59 |
| | | 3429 | | OH···O═C | 3432 | 466 |
| | | 3724 | | free OH | 3726 | 76 |
| $Cw_2$ | | 3224 | *cis*-$w_2$ | NH···water | 3208 | 300 |
| | | 3326 | | OH···C═O | 3311 | 700 |
| | | 3406 | | OH···water | 3370 | 1038 |
| | | 3714 | | free OH | 3715 | 64 |
| | | 3720 | | free OH | 3720 | 89 |
| | | 3171, 3205 | | $2\nu_2$ of $H_2O$ | | |
| $Cw_3$ | | 3204/3224 | *cis*-$w_3$(b) | NH···water | 3168 | 362 |
| | | 3314 | | 1. OH···C═O | 3262 | 1428 |
| | | 3372 | | 3. OH···water | 3410 | 327 |
| | | 3442 | | 2. OH (s) | 3465 | 435 |
| | | 3652 | | 2. OH (a) | 3659 | 97 |
| | | 3719 | | free OH | 3718 | 86 |
| | | 3719 | | free OH | 3724 | 75 |
| | | 3204/3224 | | $2\nu_2$ of $H_2O$ | | |
| dimer TC | | 3415 | *trans-cis* | c-NH···$\pi$ | 3403 | 191 |
| | | 3376 | | t-NH···O═C | 3388 | 237 |
| | | 3361, 3335 | | $2\nu_{C=O}$ | | |

[a] All frequencies calculated at B3LYP/6-31+G* level (except the dimer, which is at HF/6-31G* level). The B3LYP scaling factor is 0.977 (although 0.9742 is used for more accurate prediction of free OH bands)[13] and the HF scaling factor is 0.89.[27]

The *trans* amide presents an NH site and two alternative carbonyl sites with similar binding energies. HF/6-31G* and B3LYP/6-31+G* calculations favor one of the carbonyl bound clusters, *trans*-$w_1$(b), but at the MP2 level the NH bound structure *trans*-$w_1$(a) has a larger binding energy. The effects of weaker, secondary interactions are seen in both of these clusters. The NH···$O_{water}$ bond of *trans*-$w_1$(a) is bent 34° from linearity to allow an OH···$\pi$ interaction between water and the aromatic ring. In *trans*-$w_1$(b), the host geometry is distorted by changes in side chain torsional angles to permit an additional van der Waals interaction $O_{water}$···$HC_{ring}$ and to a lesser extent, $O_{water}$···$HC_{\alpha}$.

Similar trends are seen in the NBFA$(H_2O)_2$ clusters shown in Figure 6. The *cis-w*$_2$ cluster is easily the most stable, incorporating three linear hydrogen bonds and an arrangement which allows each molecule to be both H-bond donor and acceptor. The three most competitive *trans-w*$_2$ clusters are those in which the water dimer binds to the amide via one of the three H-bond sites. Of these, *trans*-$w_2$(a) is preferred as it benefits from a strong OH···$\pi$ bond in addition to two conventional H-bonds. The *trans*-$w_2$(b) cluster, in fashion similar to *trans*-$w_1$(b), has the host structure distorted to optimize an $O_{water}$···$HC_{ring}$ interaction. Relative energies at the MP2/6-31G*// HF/6-31G* and B3LYP/6-31G* level are given in Table 4.

**3.4. NBFA$(H_2O)_{1,2}$: Experimental Assignments.** In the mass-selected R2PI spectra of Figure 2, the most prominent feature to arise in clustering conditions is $Tw_1$ at 37640 $cm^{-1}$. Given that it appears only in the $NBFA^+$ mass channel, it might be considered either as a 1:1 hydrate or as a NBFA dimer cluster which dissociates with 100% efficiency following 1-color, 2-photon ionization. It has a vibronic spectrum very similar to the *trans* monomer, with a low-frequency $S_1$ vibration responsible for spacings of 17 $cm^{-1}$. Additional $S_1$ vibrations at 330, 437, and 537 $cm^{-1}$ mirror those seen in *trans*-NBFA (329, 433, 532 $cm^{-1}$).

The IR spectrum obtained by probing $Tw_1$ is shown in Figure 3. The band at 3720 $cm^{-1}$ is characteristic of the free OH mode of a water molecule which is a single H-bond donor. The sharp NH stretch band at 3469 $cm^{-1}$ indicates that the amide host has a *trans* conformation and also that the NH is not a hydrogen bond donor. The remaining intense, broad doublet band at 3505/ 3525 $cm^{-1}$ must be assigned to a strongly hydrogen-bonded OH oscillator OH···O═C. The doublet structure is most likely associated with a strong Fermi-resonance-type interaction with some other state. It is remarkably similar to the 3513/3536 $cm^{-1}$ doublet seen in the carbonyl-bound 1:1 hydrate of *trans*-NPF.[13] The IR data are consistent, therefore, with either of the carbonyl-bound structures, *trans*-$w_1$(b) or *trans*-$w_1$(c) in Figure 5.

**TABLE 3: Ab Initio Results for NBFA$(H_2O)_1$ Clusters[a]**

| | | | | |
|---|---|---|---|---|
| $E_{bind}$(HF)/kJ mol$^{-1}$ [b] | 19.1 | 12.4 | 13.7 | 12.4 |
| $E_{bind}$(MP2)/kJ mol$^{-1}$ [c] | 35.1 | 26.4 | 24.1 | 20.9 |
| $E_{bind}$(B3LYP)/kJ mol$^{-1}$ [d] | 31.4 | 19.3 | 23.6 | 22.2 |
| $E_{rel}$(HF)/kJ mol$^{-1}$ [b] | 0.0 | 4.5 | 1.0 | 3.5 |
| $E_{rel}$(MP2)/kJ mol$^{-1}$ [c] | 0.0 | 4.2 | 4.1 | 8.6 |
| $E_{rel}$(B3LYP)/kJ mol$^{-1}$ [d] | 0.0 | 8.1 | 3.9 | 5.3 |
| $\tau_1$ ($NC_\alpha C_1C_2$)/° | 39 | 66 | 95 | 69 |
| $\tau_2$ ($CNC_\alpha C_1$)/° | −114 | −95 | −122 | −94 |
| $\tau_3$ ($OCNC_\alpha$)/° | 177 | −7 | −3 | −5 |
| $r$ (N−H···$OH_2$)/pm | 200 | 203 | | |
| $r$ (C═O···H−OH)/pm | 193 | | 191 | 195 |
| $r$ (HO−H···$\pi C_{ortho}$)/pm | | 248 | | |
| $r$ ($H_2O$···H−$C_{ortho}$)/pm | | | 240 | |
| $r$ ($H_2O$···H−$C_{alpha}$)/pm | | | 248 | |
| $A''$/MHz | 2039.4 | 1551.4 | 1773.6 | 2307.3 |
| $B''$/MHz | 498.1 | 731.2 | 625.1 | 473.9 |
| $C''$/MHz | 480.0 | 601.5 | 503.9 | 415.2 |
| $A'$/MHz[e] | 2041.7 | 1506.6 | 1696.1 | 2244.6 |
| $B'$/MHz[e] | 492.8 | 732.0 | 635.3 | 473.0 |
| $C'$/MHz[e] | 472.7 | 590.9 | 506.8 | 413.2 |
| $\|R_e\| \times 10^{30}$/Cm[f] | 0.49 | 1.06 | 0.98 | 0.23 |
| $\mu_a^2$: $\mu_b^2$: $\mu_c^2$ [f] | 52:27:21 | 57:40:3 | 69:21:10 | 33:62:5 |
| $\theta_{elec}$/° [f] | −19 | −1 | −81 | −74 |

[a] Ground state geometric properties are from MP2/6-31G* optimizations, and binding energies are given relative to the corresponding monomer. [b] HF/6-31G* including zero point corrections scaled by 0.9. $E_{bind}$ incorporates BSSE corrections. [c] MP2/6-31G* including HF zero point corrections scaled by 0.9. $E_{bind}$ incorporates BSSE corrections on the HF component of the wave function. [d] B3LYP/6-31+G* including zero point corrections. [e] $\%\Delta A$, $\%\Delta B$, $\%\Delta C$ from CIS/6-31G* and HF/6-31G* calculations applied to MP2/6-31G* constants. [f] CIS/6-31G*. $\theta_{elec}$ is defined as the angle between the short axis of the benzene ring perpendicular to the $C_1-C_\alpha$ bond and the transition moment.

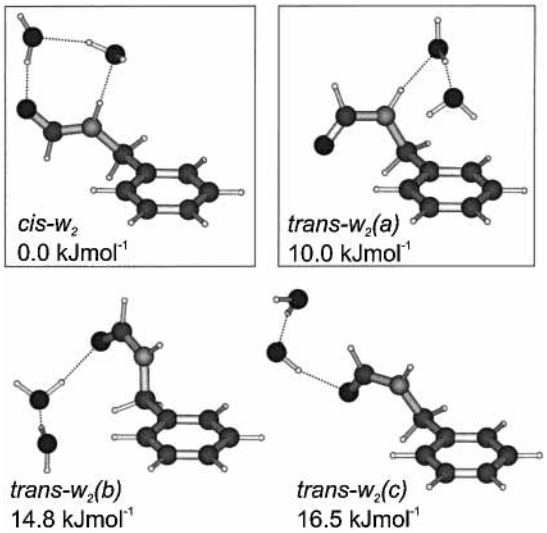


**Figure 6.** Ab initio structures for 1:2 hydrates of NBFA, together with their relative energies at the MP2/6-31G*//HF/6-31G* level. See Table 4. The enclosing boxes indicate structures that are assigned experimentally.

$Tw_1$ is the feature that dominates the fluorescence excitation spectra of Figure 4. To further clarify its structure, the partially resolved band contour shown in Figure 7 was recorded by fluorescence excitation. Simulated band contours, based on the ab initio data for *trans*-$w_1$(a),(b) and (c) given in Table 3, are also shown. The match between the experimental contour and that of *trans*-$w_1$(b) is excellent, while the *trans*-$w_1$(c) contour has insufficient a-type character. The *trans*-$w_1$(a) contour is better in this respect but is ruled out by consideration of the IR data. Examination of the partially resolved band contour of $Tw_1$, therefore, favors assignment to the *trans*-$w_1$(b) structure rather than *trans*-$w_1$(c). In support of this, HF, MP2 and B3LYP relative energies all indicate enhanced stability for *trans*-$w_1$(b) compared to *trans*-$w_1$(c) as a result of the additional $O_{water}$···HC interactions.

**TABLE 4: Ab Initio Results for NBFA$(H_2O)_2$ Clusters[a]**

| | | | | |
|---|---|---|---|---|
| $E_{rel}$(HF)/kJ mol$^{-1}$ [b] | 0.0 | 9.7 | 8.5 | 7.8 |
| $E_{rel}$(MP2)/kJ mol$^{-1}$ [c] | 0.0 | 10.0 | 14.8 | 16.4 |
| $E_{rel}$(B3LYP)/kJ mol$^{-1}$ [d] | 0.0 | 17.3 | | |
| $E_{bind}$(B3LYP)/kJ mol$^{-1}$ [d] | 73.7 | 52.5 | | |
| $\tau_1$ ($NC_\alpha C_1C_2$)/° | 49 | 67 | 98 | 63 |
| $\tau_2$ ($CNC_\alpha C_1$)/° | −122 | −97 | −171 | −148 |
| $\tau_3$ ($OCNC_\alpha$)/° | −178 | −1 | 0 | 2 |

[a] Ground state geometric properties are from HF/6-31G* optimizations. [b] HF/6-31G* including zero point corrections scaled by 0.9. [c] MP2/6-31G* including HF zero point corrections scaled by 0.9. [d] B3LYP/6-31+G* including zero point corrections.

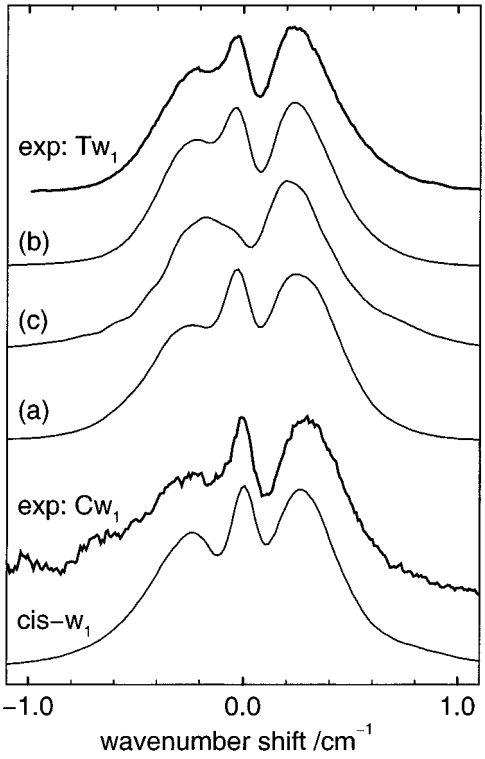


**Figure 7.** Fluorescence excitation contours of $Tw_1$ (top) and $Cw_1$ ($2^{nd}$ bottom). Also shown are simulations based on ab initio data for *trans*-$w_1$ (b), (c), (a) and *cis*-$w_1$ in Table 3, with laser line width 0.12 $cm^{-1}$ and $T_{rot}$ = 1.5 K.

The extent to which $Tw_1$ fragments in the R2PI spectra suggests that the geometry which is favored for the neutral is repulsive in the ion. A HF/6-31G* calculation on the *trans*-NBFA ion found that 80% of the Mulliken charge is carried by the amide side chain. If the amide does become positively charged as this implies, then it becomes unattractive as an H-bond acceptor for water and fragmentation is expected. Similar behavior has been observed in the hydrated clusters of phenylethylamine,[19] and benzene,[24] where water is the proton donor and the charge−permanent dipole interaction is repulsive in the ionized cluster.

The efficient dissociation of the $Tw_1$ ion highlights the difficulty in determining the number of bound solvent molecules solely on the basis of their fragmentation pattern. To help assign the stoichiometry of some the remaining clusters, their populations were measured as a function of the time delay between the signal to the pulse valve and firing the laser. The finite time required to open the valve and establish the jet expansion results

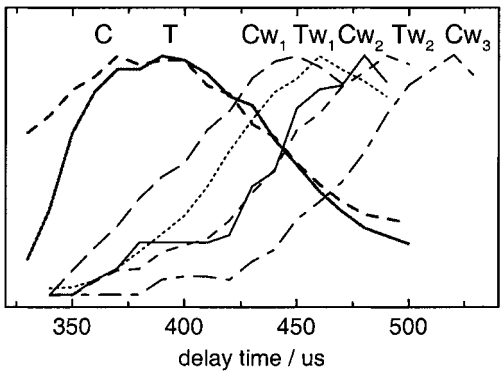


**Figure 8.** Ion signal for NBFA species, as a function of delay time between opening the pulse valve and firing the UV laser.

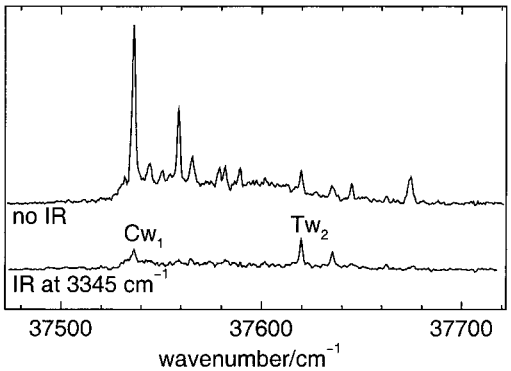


**Figure 9.** IR−UV holeburning of $Cw_1$. The R2PI spectra are recorded in the NBFA$(H_2O)_1^+$ mass channel, with the IR laser turned off (top) or fixed to 3345 $cm^{-1}$ (bottom).

in considerable variation in the species observed. The monomer features that appear in the initial period are followed by binary complexes, and then clusters which become progressively larger as time elapses. This property of a pulsed jet expansion has been used previously to assign benzyl alcohol hydrate clusters.[25] Figure 8 shows the behavior of NBFA species. The appearance of $Cw_1$ prior to $Tw_1$, together with its detection via NBFA-$(H_2O)_1^+$ ions point to a 1:1 hydrate, and probably one with a greater binding energy than $Tw_1$. This and the position of $Cw_1$ in the electronic spectrum (shifted +10 $cm^{-1}$ relative to C) suggest the *cis*-$w_1$ structure of Figure 5. The fluorescence excitation contour of $Cw_1$ in Figure 7 matches the *cis*-$w_1$ simulation well but is also similar to some of the *trans*-$w_1$ simulations. It is the IR spectrum of $Cw_1$ in Figure 3 that clinches the argument for assignment to *cis*-$w_1$. The bands at 3345 and 3429 $cm^{-1}$ correspond to the H-bonded NH···$O_{water}$ and OH···$O_{amide}$ oscillators and 3724 $cm^{-1}$ is the free OH stretch frequency of water. The B3LYP/6-31+G* frequencies for *cis*-$w_1$, given in Table 2, are in excellent agreement with these data.

The *trans* isomer of FA gives rise to two alternative 1:1 hydrates in the jet, with water bound via NH in one and C═O in the other. The R2PI spectra in Figure 9 were recorded to examine the NBFA$(H_2O)_1^+$ mass channel for signs of an alternative *trans*-NBFA cluster. The top spectrum was measured as normal, while the bottom "hole-burn" spectrum was measured with the IR laser in operation, fixed at 3345 $cm^{-1}$—resonant with the NH···$O_{water}$ band of $Cw_1$. The vibronic features associated with $Cw_1$ are greatly depleted, exposing $Tw_2$ and another weak feature separated by 16 $cm^{-1}$. Figure 8 shows that the population of $Tw_2$ grows later in the expansion than either $Cw_1$ or $Tw_1$ but has the same dependence as $Cw_2$, which appears in the NBFA$(H_2O)_2^+$ mass channel. A preliminary assignment of $Tw_2$ to a doubly hydrated cluster is confirmed

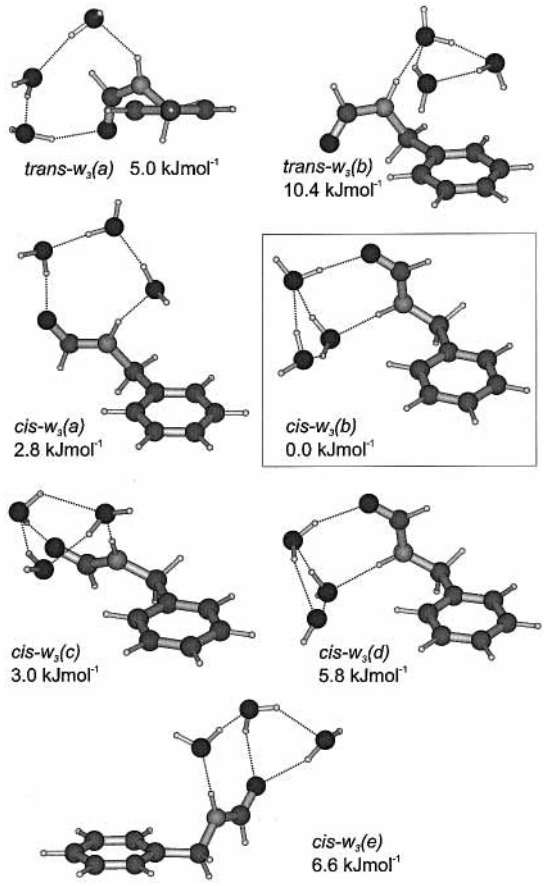


**Figure 10.** Ab initio structures for 1:3 hydrates of NBFA, together with their relative energies at the MP2/6-31G*//HF/6-31G* level. See Table 5. The enclosing box indicates the structure assigned experimentally.

by its IR spectrum, given in Figure 3. The band at 3472 $cm^{-1}$ is too wide for an unperturbed NH stretch and must therefore be assigned to a strongly H-bonded OH stretch, while the 3368 $cm^{-1}$ band is assigned to an H-bonded NH stretch and the 3593 $cm^{-1}$ band to a an OH···$\pi$ oscillator. The pattern of bands fits only the *trans*-$w_2$(a) cluster of Figure 6, in which the water dimer bridges between the amide NH and the $\pi$ system of the ring. The analogous cluster in NPF gives rise to an almost identical IR spectrum.[13] The additional feature next to $Tw_2$ in Figure 8 is assigned to a vibronic transition exciting an $S_1$ vibration of 16 $cm^{-1}$, as its IR spectrum is identical to that of $Tw_2$.

The $Cw_2$ peak appears in the NBFA$(H_2O)_2^+$ mass channel, shifted +7 $cm^{-1}$ from origin C and −3 $cm^{-1}$ from $Cw_1$. Not surprisingly, its IR spectrum supports assignment to the *cis*-$w_2$ structure of Figure 6. The OH···$O_{amide}$ and OH···$O_{water}$ bands at 3326 and 3406 $cm^{-1}$ are extremely intense and broad. The NH···$O_{water}$ stretch is assigned to the band at 3242 $cm^{-1}$, and the two bands at 3171 and 3205 $cm^{-1}$ are assigned to overtones of the $\nu_2$ bending modes of water. Frequencies close to 3200 $cm^{-1}$ are quite typical for the $2\nu_2$ mode of water hydrogen-bonded in clusters of this type.[13]

**3.5. NBFA$(H_2O)_3$: Ab Initio Results.** Seven alternative structures of NBFA$(H_2O)_3$ clusters are shown in Figure 10, together with their relative energies at the MP2/6-31G*//HF/6-31G* level. For *trans*-NBFA, a "daisy chain" of three water molecules is able to bridge between the NH and CO sites, and the *trans*-$w_3$(a) structure is preferred over *trans*-$w_3$(b), in which a cyclic water trimer bridges between the NH and the $\pi$-system of the aromatic ring. For the *cis* amide, there are several structural forms with comparable energies: the "daisy chain"

**TABLE 5: Ab Initio Results for NBFA$(H_2O)_3$ Clusters[a]**

| | | | | | | | |
|---|---|---|---|---|---|---|---|
| $E_{rel}$(HF)/kJ mol$^{-1}$ [b] | 0.0 | 1.8 | 6.1 | 8.8 | 5.4 | 3.9 | 14.5 |
| $E_{rel}$(MP2)/kJ mol$^{-1}$ [c] | 2.8 | 0.0 | 3.0 | 5.8 | 6.6 | 5.0 | 10.4 |
| $E_{rel}$(B3LYP)/kJ mol$^{-1}$ [d] | 0.0 | 7.0 | 11.8 | 14.4 | 11.4 | 11.0 | 26.3 |
| $E_{bind}$(B3LYP)/kJ mol$^{-1}$ [d] | 107.1 | 100.1 | 95.2 | 92.7 | 95.7 | 92.1 | 76.8 |
| $\tau_1$ ($NC_\alpha C_1C_2$)/° | 56 | 32 | 28 | 31 | 52 | 44 | 63 |
| $\tau_2$ ($CNC_\alpha C_1$)/° | −121 | 79 | −127 | 76 | −123 | −121 | −100 |
| $\tau_3$ ($OCNC_\alpha$)/° | −178 | −175 | −179 | −176 | −178 | −5 | 0 |
| $r$ ($H_2O\cdots H-C_{ortho}$)/pm | | 293 | 295 | 275 | | | |

[a] Ground state geometric properties are from HF/6-31G* optimizations. [b] HF/6-31G* including zero point corrections scaled by 0.9. [c] MP2/6-31G* including HF zero point corrections scaled by 0.9. [d] B3LYP/6-31+G* including zero point corrections.

structure *cis*-$w_3$(a), the "triangular water" structures *cis*-$w_3$(b)−(d) in which a cyclic water trimer is bound to both the CO and NH groups, and *cis*-$w_3$(e) in which two waters are bound to the carbonyl and one to the NH. The "triangular water" structures differ by the internal arrangement of hydrogen bonds between the water molecules. The "daisy chain" *cis*-$w_3$(a) and the "triangular water" *cis*-$w_3$(b) structures are the two lowest energy forms at each level of theory, with *cis*-$w_3$(a) more stable at the HF and B3LYP levels and *cis*-$w_3$(b) favored when electron correlation is included. There is some discrepancy in the structures of the "triangular water" structures depending on the calculation. At HF/6-31G* level, *cis*-$w_3$(b), (c) and (d) have the dihedral angles of the side chain distorted to the extent that an additional $O_{water}\cdots HC_{ring}$ interaction is allowed and in (b) and (d) the host geometry is much closer to conformer *cis** than *cis* (see Table 5). B3LYP calculations lead to structures in which there is no $O_{water}\cdots HC_{ring}$ interaction and the side chain is perturbed to a lesser extent. In addition, the *cis*-$w_3$(c) structure relaxes into the "daisy chain" form, *cis*-$w_3$(a). MP2/6-31G* optimization of *cis*-$w_3$(b) results in a structure ($\tau_1 = 24°$, $\tau_2 = 85°$, $r_{Owater\cdots HCring} = 251$ pm) consistent with the HF calculation and 4 kJ mol$^{-1}$ more stable than the MP2 optimized *cis*-$w_3$(a) cluster.

**3.6. NBFA$(H_2O)_3$: Experimental Results.** The dominant feature in the NBFA$(H_2O)_3^+$ mass channel, labeled $Cw_3$ in Figure 2, is also present in the NBFA$(H_2O)_2^+$ mass channel as a result of partial fragmentation of the parent ion. It is shifted +166 cm$^{-1}$ from origin T and +240 cm$^{-1}$ from origin C. Such a shift is too large be explained by simple solvation of the amide since it is electronically "isolated" from the ring by the methylene group. It implies considerable perturbation in the geometry of the host.

The IR spectrum obtained by probing $Cw_3$ is shown in Figure 3. It is similar in general appearance to the spectrum of $Cw_2$, except for the distinctive, broad band at 3652 cm$^{-1}$. Its slightly unusual appearance results from dips in IR laser power at 3647 cm$^{-1}$, 3649, 3651, and 3653 cm$^{-1}$ caused by strong absorption lines of atmospheric water.[26] The symmetric stretch of a water molecule which is H-bonded only as an acceptor appears in this region, but such bands are weak, narrow and accompanied by the antisymmetric stretch at ca. 3750 cm$^{-1}$.[13] The only feasible assignment of the 3652 cm$^{-1}$ band is to the "antisymmetric" OH stretch mode of a water molecule that is a double H-bond donor. When the two acceptors are equivalent, the symmetric and antisymmetric OH stretch modes are red-shifted relative to the water molecule but remain separated by ca. 100 cm$^{-1}$, as was illustrated in the spectra of benzene$(H_2O)_8$ complexes.[17] If a water molecule is a single donor only, the "free OH" band appears as a narrow transition around 3710−3730 cm$^{-1}$. The pattern in the spectrum of $Cw_3$ represents an intermediate case in which one of the water molecules is bound to two acceptors that are not equivalent. The "daisy chain" structures *trans*-$w_3$(a) and *cis*-$w_3$(a) may be eliminated immediately. Comparison of the IR spectrum of $Cw_3$ with those

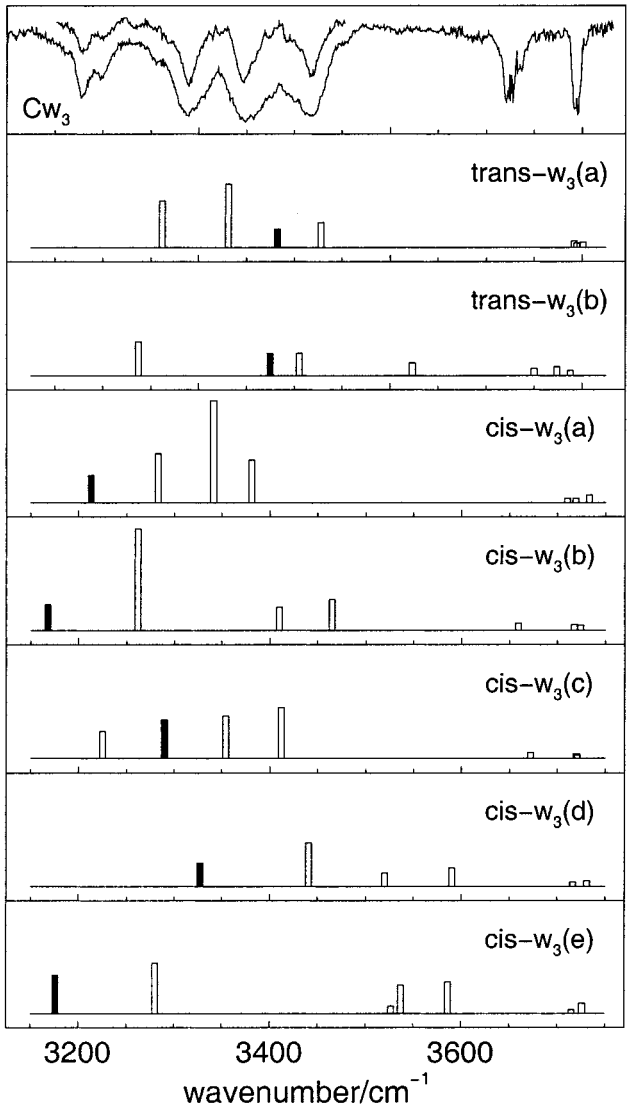


**Figure 11.** IR−UV ion depletion spectrum probing electronic origin band $Cw_3$. The stick spectra shown below are based on B3LYP/6-31+G* results, using scaling factor 0.977 (and 0.9742 for free OH). To obtain frequencies for *cis*-$w_1$(c), the O···O distance of the waters attached to NH and CO groups was fixed at 3.0 Å.

predicted at the B3LYP/6-31+G* level further narrows the choice of feasible candidates to the "triangular water" structures *cis*-$w_3$(b) and (c); see Figure 11. The perturbed side chains of these structures are also consistent with the highly shifted electronic origin of $Cw_3$. Calculated relative energies unanimously support assignment to *cis*-$w_3$(b) rather than *cis*-$w_3$(c). Minor discrepancies between the experimental and simulated spectra are not surprising. First, the calculated shifts in NH stretch frequencies are overestimated in all the other NH bound clusters of NBFA and NPF. Second, the B3LYP structure does

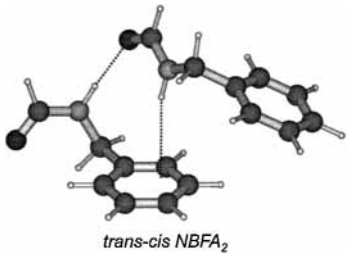


**Figure 12.** Ab initio (HF/6-31G*) structure of the heterodimer *trans*/*cis*-$NBFA_2$.

not account for the $O_{water}\cdots HC_{ring}$ interaction, which must affect the coupling of bound OH stretch frequencies to some extent. This interaction appears to be necessary for a triangular water structure to be favored over the daisy chain arrangement, and presumably it is this interaction that the causes the relaxation of conformer *cis* into *cis** upon cluster formation.

**3.7. $NBFA(H_2O)_{4,5}$.** It is quite possible that some of the very weak features in the R2PI spectra of the $NBFA(H_2O)_2^+$ and $NBFA(H_2O)_3^+$ mass channels are associated with alternative $n = 3$ clusters (e.g., of *trans*-NBFA), but they are too weak to be examined by IR spectroscopy. The second strongest feature in the $NBFA(H_2O)_3^+$ mass channel, however, shifted just $-11$ $cm^{-1}$ from $Cw_3$ also appears in the $NBFA(H_2O)_4$ mass channel. Its position in the spectrum suggests assignment to a 1:4 hydrate with similar structure to *cis*-$w_3$(b), i.e., a *cis** conformation of the host, bound to a cyclic water tetramer via NH and C═O groups. Confirmation of this structure through IR/UV spectroscopy was not possible as a result of the low signal levels. Two further peaks are evident in the $NBFA(H_2O)_4$ mass channel, in positions close to the known *cis* and *trans* hydrate origins. They are most likely associated with 1:5 hydrates, with the amide host taking up *cis* and *trans* conformations.

**3.8. $NBFA_2$.** The R2PI spectrum measured in the dimer mass channel is shown in Figure 2. The most prominent feature in the origin region, labeled TC, is shifted $-10$ $cm^{-1}$ relative to origin C. Its IR spectrum, given in Figure 3, reveals that both NH groups are hydrogen bonded as there is no sign of unperturbed NH stretch bands. The sharp band at 3415 $cm^{-1}$ is indicative of a weak hydrogen bond, e.g. NH$\cdots\pi$ or a strained NH$\cdots$O, while the intense, broad band at 3376 $cm^{-1}$ suggests a strong NH$\cdots$O═C hydrogen bond. The only structure consistent with these observations is a heterodimer composed of *cis* and *trans*-NBFA, such as the one shown in Figure 12. The 3415 $cm^{-1}$ band is assigned to the NH stretch of *cis*-NBFA, red-shifted 28 $cm^{-1}$ by H-bonding to the aromatic ring of *trans*-NBFA. The band at 3376 $cm^{-1}$ is the NH stretch of *trans*-NBFA, red-shifted 102 $cm^{-1}$ by H-bonding to the carbonyl oxygen of *cis*-NBFA. The corresponding shifts at the HF/6-31G* level, 22 and 67 $cm^{-1}$, are underpredicted as usual.[27] Two weaker features at 3361 and 3335 $cm^{-1}$ are most likely associated with carbonyl overtones. The HF/6-31G* calculation indicates that the carbonyl stretches within the TC dimer are highly coupled and red-shifted an average of 24 $cm^{-1}$ relative to the carbonyl stretch frequencies of *cis* and *trans*-NBFA. The IR bands assigned to the carbonyl *overtones* are red-shifted an average of 102 $cm^{-1}$ from the monomer carbonyl overtones. Such large shifts for the overtones are consistent with the more anharmonic potential induced by H-bonding to the carbonyl.

Given its position in the electronic spectrum, it is reasonable to assume that TC is the origin associated with excitation of the *cis*-amide within the dimer. A series of closely spaced vibronic transitions are also observed in the $NBFA_2^+$ mass channel, blue-shifted slightly from the *trans*-NBFA origin. This is where the origin associated with excitation of the *trans* isomer is expected, although it is possible that these some or all of these transitions belong to an alternative dimer consisting of two *trans*-NBFA molecules.

## 4. Discussion and Conclusions

**4.1. Structure.** The discriminating power provided by IR spectroscopy has made it possible to contrast the manner in which water binds to *cis* and *trans* isomers of the NBFA molecule. The *cis* amide forms cyclic H-bonded structures with one or two water molecules, binding via strong H-bonds to the neighboring C═O and NH groups. With the addition of a third water molecule, the cyclic water trimer binds to both these groups in preference to a linear chain of three waters. For *trans*-NBFA, a single water binds to the carbonyl group while two waters bind to the NH group instead.

In these hydrates, every water molecule is acting as both donor and acceptor. In the case of *trans*-NBFA, the additional bond is either an OH$\cdots\pi$ H-bond ($Tw_2$) or involves a dispersive type interaction $O_{water}\cdots$HC ($Tw_1$). These secondary interactions play a key role in selecting which of several competing structures is energetically favored in the jet expansion. There is also growing recognition of the importance of such "weak interactions" as OH$\cdots\pi$, CH$\cdots$O, CH$\cdots\pi$ in protein structure,[28−32] and consequently in drug design.[33,34] In crystallography studies, the peptide $C_\alpha$-H group is the most frequent donor in CH$\cdots$O contacts, consistent with its polarization by adjacent electron-withdrawing C═O and NH groups. Carbonyl groups are a common donor, binding to neighboring $C_{(i)}H_\alpha$ and $N_{(i+1)}H$ groups via its two lone pairs.[28] CH$\cdots$O interactions are also found when water is bound within proteins, taking up some of the available acceptor sites of water not involved in conventional H-bonds.[30] The arrangement of water within $Tw_1$ raises the question of whether some of the waters bound to $C{=}O_{(i)}$ within proteins might have a tendency to interact with the adjacent $C_{(i+1)}H$ groups, thereby contributing additional stability to the H-bond. For water to bind in this manner, the optimal value of the Ramachandran angle $\phi$ ($CC_\alpha NC$) is $\pm 120°$ which coincides well with the range of sterically allowed angles.[35]

In the *trans*-NBFA hydrates, the flexibility of the amide side chain host plays a key role in promoting the additional interactions. The angle $\tau_2$ ($C_1C_\alpha NC$) is equivalent to the Ramachandran angle $\phi$, the flexibility of which is crucial in proteins. The geometry of the *trans*-NBFA side chain ($\tau_1 = 71°$, $\tau_2 = -92°$) is almost unaltered in *trans*-$w_1$(a) and (c), but in *trans*-$w_1$(b), it undergoes considerable distortion ($\tau_1 = 95°$, $\tau_2 = -122°$) to facilitate the $O_{water}\cdots$HC interactions. In the equivalent two water cluster, *trans*-$w_2$(b), the distortion is even greater ($\tau_1 = 98°$, $\tau_2 = -171°$). This illustrates very well the low barriers to rotation about $\tau_2$, given that the $O_{water}\cdots$HC interactions amount to only a few kJ $mol^{-1}$. Peptides consisting of glycine residues have similar flexibility, while the bulkier side groups of other amino acids sterically limit the Ramachandran angles $\phi$ and $\theta$.[35] In the case of the $Cw_3$ cluster, the weak $O_{water}\cdots$HC interaction affects both the arrangement of water molecules and the geometry of the host. In 2-phenylacetamide, three waters bind in a "daisy chain" fashion.[36] While the equivalent structure for *cis*-NBFA is very competitive energetically (see Table 5), experimentally *cis*-$w_3$(b) (see Figure 10) is the one chosen. In this structure, the amide side chain apparently adopts the *cis** conformation, despite the fact that it is 6 kJ $mol^{-1}$ less stable in the absence of water molecules.

**4.2. Cluster Formation.** The pattern of NBFA clusters detected, and how their populations vary with delay time, give some insight concerning the pathway for cluster formation in the jet. The data in Figure 8 show that *cis*-NBFA forms a 1:1 hydrate ca. 20 $\mu$s earlier than *trans*-NBFA, suggesting a strong dependence on binding energy. In considering 1:2 hydrates, the pathways that must be considered are, first, formation of a water dimer (1a) followed by complexation with the amide (1b) and, second, formation of a suitable 1:1 complex (2a) followed by addition of the second water molecule (2b). The observation of only carbonyl-bound 1:1 hydrates of *trans*-NBFA and NH-bound 1:2 hydrates favors the first pathway, and the simultaneous formation of $Cw_2$ and $Tw_2$ in Figure 8 supports this. The binding energies corresponding to steps (1b), (2a) and (2b) are all markedly different for the *cis* and *trans* amides. If (1a) is the step which limits cluster formation, however, then the 1:2 hydrates of *cis* and *trans*-NBFA should appear at the same stage. Whatever the mechanisms, the result is considerable changes in the *cis*/*trans* ratio as the number of water molecules increases. The monomer and 1:1 hydrates are dominated by *trans*-NBFA, while the $n = 2-4$ hydrates are comprised mostly of *cis*-NBFA. In the $n = 5$ hydrates, the balance appears to be restored, but assignment of these clusters is only tentative. Similar conformationally dependent clustering behavior has also been observed in other systems, e.g., 2-amino-1-phenylethanol,[7] 2-phenylethylamine[19,37] and amphetamine.[37]

**4.3. IR Spectroscopy.** Many of the trends observed in the IR spectra of Figure 3 were mirrored in NPF. There is a strong correlation between H-bond strength, the red-shift of IR stretch frequencies and their bandwidth. The broadest IR bands, for example, are those of $Cw_2$, in which strong, linear H-bonds link the water dimer to C═O and NH groups and cooperative effects are maximized since each molecule acts as both donor and acceptor. This broadening is generally attributed to anharmonic coupling with the vibrational bath, which is greatly enhanced in the OH or NH group by H-bond formation.[38] It can be an aid to spectral assignment, e.g., the width of the $Cw_1$ band at 3429 $cm^{-1}$ is characteristic of an H-bonded OH stretch rather than a slightly shifted NH stretch mode. Particularly in the clusters with broad IR bands, the ab initio calculations also indicate coupling of the H-bonded stretch modes, resulting in distribution of vibrational motion along the H-bonded chain.

Shifts in NH frequencies reveal the relative strengths of different acceptors. The relationship between NH shift and H-bond strength is clearly not linear, but there is a strong correlation. The red-shift found for the *cis*-NH$\cdots\pi$ bond within the TC dimer is small (28 $cm^{-1}$), but the H-bond character is still evident. The *trans* NH$\cdots$O═C bond within the dimer, an excellent model for peptide interactions, results in a red-shift of 102 $cm^{-1}$. The NH$\cdots O_{water}$ bond in *trans*-NPF$(H_2O)_1$ gives a −61 $cm^{-1}$ shift, while the 1:2 hydrates of *trans*-NPF and *trans*-NBFA where $(H_2O)_2$ bridges between the amide NH and $\pi$-system of the ring show shifts of −94 $cm^{-1}$ and −107 $cm^{-1}$. The larger red-shifts for the $(H_2O)_2$ complexes, compared to a single water acceptor, result from cooperative strengthening of the NH$\cdots O_{water}$ bond. A similar phenomenon is seen in the H-bond *donating* ability of $(H_2O)_2$ compared to $H_2O$ in complexes with benzene.[39] The amide carbonyl group is therefore a stronger H-bond acceptor than a single water molecule, but on a par with the water dimer. The large shift in the NH stretch frequency of $Cw_1$ (−98 $cm^{-1}$), despite its nonlinear NH$\cdots$O bond, again indicates cooperative strengthening as each molecule is both H-bond acceptor and an H-bond donor. These effects are further enhanced in $Cw_2$ (shift −201 $cm^{-1}$) with its strong, linear H-bonds and in $Cw_3$ (shift −219 $cm^{-1}$), where the water molecule bound to NH is a double donor.

**4.4. Photophysics.** The fluorescence spectra of NBFA given in Figure 4 are unusual in that they are dominated by the cluster species. The $S_1$ state of the *trans* conformer is affected by a competing, nonfluorescent process with a lifetime of ca. 20−25 ns, dramatically affecting the fluorescence yield. Presumably it is also active in the *cis* conformer for which no fluorescence is detected. The binding of water molecules or another NBFA molecule to either conformer disrupts this process. In some cases, $Tw_1$ or $Cw_3$ for example, the bound species induces significant geometric changes in the amide side chain. In others, like $Cw_1$ and $Cw_2$, there is very little perturbation in the geometry, and the $S_1 \leftarrow S_0$ origin is almost unshifted. This suggests that the competing nonfluorescent process may involve an accidental resonance leading to triplet interconversion or radiationless relaxation. What is unusual, however, is that 2-phenylacetamide displays similar behavior in that the molecule itself does not fluoresce, while its clusters do.[36] Apparently the solvation induced change is quite subtle, yet it has a large effect on the fluorescence properties of the benzene chromophore.

**Acknowledgment.** We are grateful to the Leverhulme Trust for postdoctoral support (E.G.R.) and to the EPSRC for grant support and a studentship (M.R.H.). We thank the EPSRC Laser Support Facility for the loan of the LAS laser system employed in R2PI experiments.

## References and Notes

(1) Austin, J. C.; Jordan, T.; Spiro, T. G. In *Biomolecular Spectroscopy Part A*; Clark, R. J. H., Hester, R. E., Eds.; John Wiley & Sons: Chichester, U.K., 1993; p55.

(2) Zwier, T. S. *Annu. Rev. Phys. Chem*. **1996**, *47*, 205.

(3) Ebata, T.; Fujii, A.; Mikami, N. *Int. Rev. Phys. Chem*. **1988**, *17*, 331.

(4) Mons, M.; Robertson, E. G.; Snoek, L. C.; Simons, J. P. *Chem. Phys. Lett*. **1999**, *310*, 423.

(5) Mons, M.; Robertson, E. G.; Simons, J. P. *J. Phys. Chem. A* **2000**, *104*, 1430.

(6) Snoek L. C.; Robertson, E. G.; Kroemer, R. T.; Simons, J. P. *Chem. Phys. Lett*. **2000**, *321*, 49.

(7) Graham, R. J.; Kroemer, R. T.; Mons, M.; Robertson, E. G.; Snoek, L. C.; Simons, J. P. *J. Phys. Chem. A* **1999**, *103*, 9706.

(8) Butz, P.; Kroemer, R. T.; Macleod, N. A.; Simons, J. P. *J. Phys. Chem. A.*, in press.

(9) Butz, P.; Kroemer, R. T.; Macleod, N. A.; Robertson, E. G.; Simons, J. P. *J. Phys. Chem. A.*, in press.

(10) Matsuda, Y.; Ebata, T.; Mikami, N. *J. Chem. Phys*. **1999**, *110*, 8397.

(11) Florio, G. M.; Gruenloh, C. J.; Zwier, T. S. *Abstr. Pap. Am. Chem*. **1999**, S218−U282.

(12) Held, A.; Pratt, D. W. *J. Am. Chem. Soc*. **1993**, *115*, 9708.

(13) Robertson, E. G. *Chem. Phys. Lett*. **2000**, *325*, 299.

(14) Dickinson, J. A.; Hockridge, M. R.; Robertson, E. G.; Simons, J. P. *J. Phys. Chem. A* **1999**, *103*, 6938.

(15) Fedorov, A. V.; Cable, J. R. *J. Phys. Chem. A* **2000**, *104*, 4943.

(16) Frisch, M. J.; Trucks, G. W.; Schlegel, H. B.; Gill, P. M. W.; Johnson, B. G.; Robb, M. A.; Cheeseman, J. R.; Keith, T.; Petersson, G. A.; Montgomery, J. A.; Raghavachari, K.; Al-Laham, M. A.; Zakrzewski, V. G.; Ortiz, J. V.; Foresman, B.; Cioslowski, J.; Stefanov, B. B.; Nanayakkara, A.; Challacombe, M.; Peng, C. Y.; Ayala, P. Y.; Chen, W.; Wong, M. W.; Andres, J. L.; Replogle, E. S.; Gomperts, R.; Martin, R. L.; Fox, D. J.; Binkley, J. S.; Defrees, D. J.; Baker, J.; Stewart, J. P.; Head-Gordon, M.: Gonzalez, C. and Pople, J. A. *Gaussian 94*, Revision D.4; Gaussian: Pittsburgh, PA, 1995.

(17) Gruenloh, C. J.; Carney, J. R.; Hagemeister, F. C.; Arrington, C. A.; Zwier, T. S.; Fredericks, S. Y.; Wood, J. T.; Jordan, K. D. *J. Chem. Phys*. **1998**, *109*, 6601.

(18) Xantheas, S. S. *J. Chem. Phys*. **1996**, *104*, 8821.

(19) Hockridge, M. R.; Robertson, E. G. *J. Phys. Chem. A* **1999**, *103*, 3618.

(20) Jadzyn, J.; Pralat, K.; Kedziora, P. *J. Phys. Chem*. **1986**, *90*, 2781.

(21) Mallard, W. G., Linstrom, P. J., Eds. Infrared and Mass spectra. In NIST chemistry webbook. NIST standard reference database no. 69. 2000, (http://webbook.nist.gov).

(22) Martinez, M. J.; Alfano, J. C.; Levy, D. H. *J. Mol. Spectrosc*. **1993**, *158*, 82.

(23) Kroemer, R. T.; Liedl, K. R.; Dickinson, J. A.; Robertson, E. G.; Simons, J. P.; Borst, D. R.; Pratt, D. W. *J. Am. Chem. Soc*. **1998**, *120*, 12573.

(24) Gotch, A. J.; Zwier, T. S. *J. Chem. Phys*. **1992**, *96*, 3388.

(25) Im, H.-S.; Bernstein, E. R.; Secor, H. V.; Seeman, J. I. *J. Am. Chem. Soc*. **1991**, *113*, 4422.

(26) Camy-Peyret, C.; Flaud, J. M.; Guelachvili, G.; Amiot, C. *Mol. Phys*. **1973**, *26*, 825.

(27) Watanabe, H.; Iwata, S. *J. Chem. Phys*. **1996**, *105*, 420.

(28) Fabiola, G. F.; Krishnaswamy, S.; Nagarajan, V.; Pattabhi, V. *Acta Crystallogr. D* **1997**, *53*, 316.

(29) Jeffrey, G. A.; Saenger, W. *Hydrogen Bonding in Biological Structures*; Springer-Verlag: Berlin, 1991; Chapter 10.

(30) Saenger, W.; Steiner, T. *J. Am. Chem. Soc*. **1993**, *115*, 4540.

(31) Starikov, E. B.; Saenger, W.; Steiner, T. *Carbohydr. Res.* **1998**, *307*, 343.

(32) Vargas, R.; Garza, J.; Dixon, D. A.; Hay, B. P. *J. Am. Chem. Soc*. **2000**, *122*, 4750.

(33) Bradley, D. *New Sci*. **1996**, *2059*, 22.

(34) Engh, R. A.; Brandstetter, H.; Sucher, G.; Eichinger, A.; Baumann, U.; Bode, W.; Huber, R.; Poll, T.; Rudolph, R.; vonderSaal, W. *Structure* **1996**, *4*, 1353.

(35) Alberts, B.; Bray, D.; Lweis, L.; Raff, M.; Roberts, K.; Watson, J. D. *Molecular Biology of the Cell*; Garland Publishing Inc.: New York, 1983.

(36) Robertson, E. G.; Hockridge, M. R.; Jelfs, P. D.; Simons, J. P. Submitted to *Phys. Chem. Chem. Phys.*

(37) Yao, J.; Im, H. S.; Foltin, M.; Bernstein, E. R. *J. Phys. Chem. A* **2000**, *104*, 6197.

(38) Blaise, P.; Henri-Rousseau, O. *Chem. Phys*. **2000**, *256*, 85.

(39) Fredericks, S. Y.; Jordan, K. D.; Zwier, T. S. *J. Phys. Chem*. **1996**, *100*, 7810.